

ProsMAE: Multi-Source MAE Pretraining for ISUP Grade Classification

Anna Jung
Seoul National University
annajung227@snu.ac.kr

Kyeonghun Kim
OUTTA
kyeonghun.kim@outta.ai

Youngung Han
Seoul National University
yuhan@snu.ac.kr

Eunseob Choi
GIST
eunseobchoi@gm.gist.ac.kr

Jiwon Yang
Seoul National University
jwyang29@snu.ac.kr

Ken Ying-Kai Liao
NVIDIA
kenyingkail@nvidia.com

Hyuk-Jae Lee
Seoul National University
hjlee@capp.snu.ac.kr

Nam-Joon Kim[†]
Seoul National University
knj01@snu.ac.kr

Abstract—Whole slide images (WSIs) provide rich diagnostic information for computational pathology, but their gigapixel scale, stain variation, scanner differences, tissue artifacts, and limited expert annotation make robust model training challenging. This paper presents a multi-source Masked Autoencoder (MAE) framework, named ProsMAE, for histopathology representation learning. Tiles from Prostate cANcer graDe Assessment (PANDA), Cancer METastases in LYmph nOdes challeNge 2017 (CAMELYON17), and BReAst Carcinoma Subtyping (BRACS) are used for ProsMAE pretraining to expose the encoder to diverse tissue morphology and acquisition conditions. The learned encoder is transferred for International Society of Urological Pathology (ISUP) grade classification through ProsCLS, using a frozen encoder and a linear classification head. ProsMAE achieved a higher mean validation quadratic weighted kappa (QWK) than the vanilla MAE frozen linear-probe baseline under the evaluated disjoint PANDA split. Repeated-split evaluation remains necessary to further establish robustness across split compositions.

Index Terms—Whole slide image analysis, self-supervised representation learning, Gleason grading, prostate cancer diagnosis, digital pathology

I. INTRODUCTION

Whole slide images (WSIs) are central to computational pathology because they preserve tissue morphology at high resolution. However, their gigapixel scale makes direct processing computationally difficult, so most pipelines rely on tile-based analysis and slide-level aggregation to connect local tissue patterns with diagnostic labels [1]–[3]. In prostate cancer, this is important because International Society of Urological Pathology (ISUP) grading depends on glandular architecture and morphological patterns that may appear only in limited biopsy regions [4].

Supervised WSI learning is limited by expensive expert annotation and weak alignment between slide-level labels and local tissue morphology [2], [3]. Self-supervised learning helps address this by learning transferable representations from unlabeled pathology tiles before downstream classification [5], [6]. Among these methods, Masked Autoencoders (MAEs) are particularly suitable because they reconstruct missing image

patches from visible tissue context using Vision Transformer (ViT) patch tokens [7], [8].

A major remaining challenge is domain variation caused by differences in scanners, staining protocols, compression, and tissue preparation [9], [10]. To improve robustness, we propose ProsMAE, a multi-source MAE pretraining framework. By pretraining on Prostate cANcer graDe Assessment (PANDA), Cancer METastases in LYmph nOdes challeNge 2017 (CAMELYON17), and BReAst Carcinoma Subtyping (BRACS) with a high mask ratio, the encoder learns morphology-preserving features that are less sensitive to dataset-specific variation [4], [11], [12].

The main contributions are summarized as follows:

- We propose ProsMAE, a multi-source MAE pretraining framework for WSI representation learning.
- We use PANDA, BRACS, and CAMELYON17 for diverse histopathology pretraining.
- We transfer the encoder to frozen linear-probe ISUP grade classification through ProsCLS.

II. METHODOLOGY

The proposed framework consists of two stages: ProsMAE, the multi-source MAE pretraining stage, and ProsCLS, the downstream ISUP grade classification stage.

TABLE I
EXTERNAL DATA SOURCE RESULTS

Setting	Best QWK	Std
PANDA-only	0.3757	0.0204
PANDA+CAMELYON17	0.4165	0.0339
PANDA+BRACS	0.4330	0.0584
PANDA+CAMELYON17+BRACS	0.4734	0.0104

As shown in Table I, three public histopathology datasets are used for representation learning: PANDA for prostate cancer, CAMELYON17 for lymph node metastasis, and BRACS for breast cancer subtype. PANDA also serves as our downstream evaluation cohort. The downstream task is formulated as a six-class classification, where Class 0 denotes benign/no-cancer biopsies and Classes 1-5 denote ISUP grade groups 1-5.

[†] Corresponding author

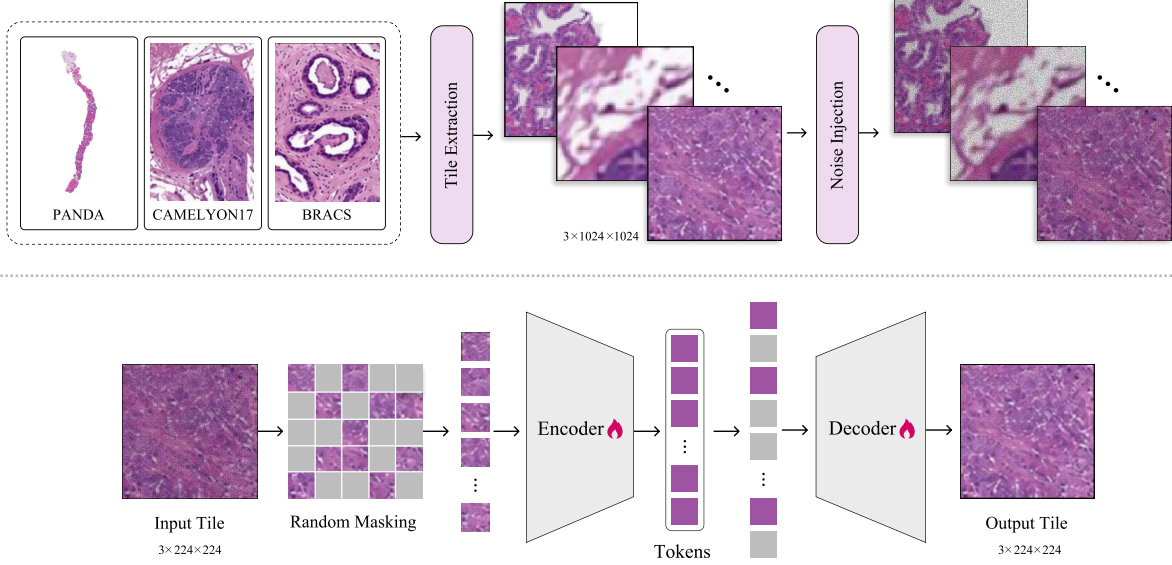


Fig. 1. ProsMAE pretraining workflow. WSI tiles from PANDA, CAMELYON17, and BRACS are randomly masked, encoded, and reconstructed to learn multi-source histopathology representations.

A. Masked Autoencoder Backbone

In the first stage, a pretrained MAE is adapted to unlabeled tiles from these three datasets via masked image reconstruction as shown in Fig. 1. Following the standard MAE design [7], the masking ratio is set to 0.75. ViTs divide each tile into fixed-size patches and process the resulting patch embeddings as a token sequence [8]. The encoder processes only visible patch tokens, while the decoder reconstructs masked regions from latent representations and mask tokens.

B. Noise Injection Ablation

Gaussian noise is added to the input before masked reconstruction while the target remains the original clean image. This ablation tests whether reconstructing from corrupted inputs improves representation robustness against typical clinical variations like scanner differences, blur, and stain variability [10], [13]. Given an input tile x , a Gaussian noise transformation $\mathcal{N}_\sigma(\cdot)$ produces:

$$\tilde{x} = \mathcal{N}_\sigma(x), \quad (1)$$

where σ denotes the noise standard deviation. We evaluate noise levels $\sigma \in \{0.02, 0.05, 0.10, 0.20\}$. The noisy tile \tilde{x} is divided into non-overlapping patches, randomly masked, and reconstructed.

The reconstruction target is the original normalized image patch values. The MAE reconstruction loss is computed over the masked patches:

$$\mathcal{L}_{MAE} = \frac{1}{|\Omega|} \sum_{i \in \Omega} \|x_i - \hat{x}_i\|_2^2, \quad (2)$$

where Ω is the set of masked patches, x_i is the target patch, and \hat{x}_i is the reconstructed patch.

C. ISUP Grade Classification

After MAE pretraining, the decoder is removed and the encoder is transferred to ProsCLS for PANDA ISUP grade classification as shown in Fig. 2. This follows the standard linear evaluation setting in self-supervised learning, where a lightweight classifier is trained on learned representations to assess feature quality [7], [14], [15].

For a slide containing N sampled tiles $\{x_1, x_2, \dots, x_N\}$, the encoder extracts a feature vector from each tile:

$$z_i = f_\theta(x_i), \quad i = 1, 2, \dots, N \quad (3)$$

where f_θ denotes the pretrained MAE encoder.

The tile-level features are aggregated into a slide-level representation using mean pooling:

$$z_{slide} = \frac{1}{N} \sum_{i=1}^N z_i \quad (4)$$

A linear classification head predicts the ISUP grade label:

$$\hat{y} = \text{Softmax}(Wz_{slide} + b). \quad (5)$$

The classifier is trained using cross-entropy loss:

$$\mathcal{L}_{cls} = - \sum_{c=1}^C y_c \log(\hat{y}_c), \quad (6)$$

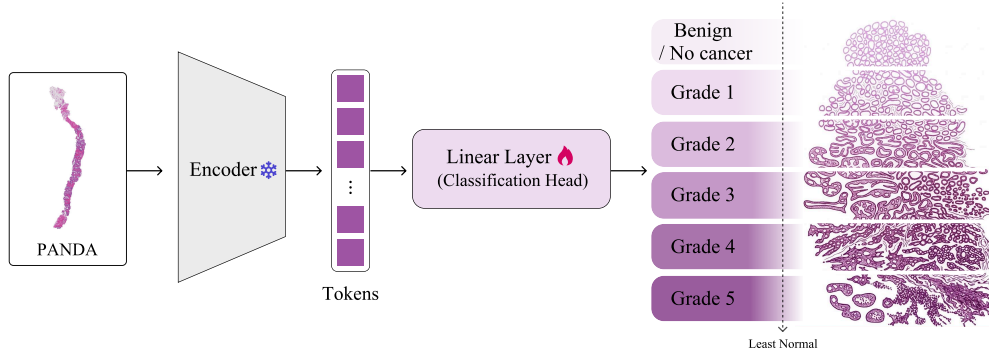


Fig. 2. ProsCLS downstream classification workflow. PANDA WSIs are divided into tiles, features are extracted using the frozen ProsMAE encoder, tile-level features are aggregated by mean pooling, and a linear classification head predicts the downstream six-class label (Benign/No cancer + ISUP Grades 1-5).

where $C = 6$ is the number of downstream classes, including ISUP Grades 1-5 and the additional benign/no-cancer class.

III. EXPERIMENTS

A. Experimental Setup

The experiments evaluate whether multi-source MAE pretraining improves downstream ISUP classification. We initialize the backbone with Facebook/Meta ViT-MAE-Base weights (ViT-B/16, ImageNet-1K pretrained) [7]. The main ProsMAE pretraining uses a mask ratio of 0.75 without added noise.

To prevent data leakage, a disjoint PANDA split is maintained: 241 slides for pretraining, 82 for downstream training, and 80 for downstream validation. WSIs were first divided into 1024×1024 tissue regions from the Level 2 downsampled image ($\approx 8.0 \mu\text{m}/\text{pixel}$ in our preprocessing setting). For MAE pretraining, these regions were resized to 224×224 before ViT patch tokenization. For downstream evaluation, 512×512 tiles were extracted and resized to 224×224 before encoder feature extraction. Stain normalization was omitted to preserve original stain variations, allowing the encoder to learn morphology under heterogeneous acquisition conditions [9], [10]. Pretraining ran for up to 5000 steps (capped at 20 epochs) using AdamW (batch size 64, learning rate 5×10^{-5}), with a 250-step warmup and cosine learning-rate decay. Each WSI contributed 100 tiles. For downstream evaluation, the encoder is frozen and a linear classification head is trained with balanced class weights using mean-pooled features of 100 tiles per slide.

B. Evaluation Metrics

Performance is evaluated using accuracy, macro F1-score, and quadratic weighted kappa (QWK) [16], a weighted agreement metric that penalizes larger ordinal disagreements more strongly. Macro F1-score computes F1 for each class independently and averages them equally, providing a more balanced evaluation across common and minority grades [17]. QWK is used because ISUP grades are ordinal, where errors between adjacent grades are less severe than errors between distant grades [4].

C. Reconstruction Performance

We evaluate the pretraining reconstruction performance of ProsMAE and compare it against standard Autoencoder (AE), Variational Autoencoder (VAE), and single-source Masked Autoencoder (MAE) baselines. Evaluations are conducted across PANDA, CAMELYON17, BRACS, as well as the combined multi-source dataset. Reconstruction quality is assessed using Learned Perceptual Image Patch Similarity (LPIPS), Structural Similarity Index Measure (SSIM), and Peak Signal-to-Noise Ratio (PSNR). We additionally record total pretraining GPU hours to compare computational efficiency.

TABLE II
PERFORMANCE COMPARISON OF THE PROSMAE MODEL AND BASELINE MODELS ON RECONSTRUCTION PERFORMANCE.

Dataset	Model	LPIPS ↓	SSIM ↑	PSNR ↑
PANDA	AE	0.065	0.6921	30.058
	VAE	0.063	0.7030	30.173
	MAE	0.061	0.7290	30.242
	ProsMAE	0.059	0.7430	31.142
CAMELYON17	AE	0.067	0.7250	31.391
	VAE	0.064	0.7270	31.423
	MAE	0.065	0.7310	31.519
	ProsMAE	0.061	0.7330	31.771
BRACS	AE	0.059	0.7310	30.833
	VAE	0.057	0.7430	30.821
	MAE	0.057	0.7420	30.923
	ProsMAE	0.056	0.7520	32.271
PANDA+BRACS +CAMELYON17	AE	0.071	0.7220	29.613
	VAE	0.069	0.7270	29.711
	MAE	0.069	0.7310	29.687
	ProsMAE	0.068	0.7330	30.006

As shown in Table II, ProsMAE achieves the best reconstruction scores among the evaluated models across the reported datasets and metrics. On the combined PANDA+BRACS+CAMELYON17 dataset, ProsMAE achieves a superior LPIPS of 0.068, SSIM of 0.7330, and PSNR of 30.006. Furthermore, ProsMAE maintains highly

competitive pretraining efficiency, requiring only 10-11 hours of GPU training time, which is faster than standard AE/VAE and comparable to vanilla MAE, suggesting the effectiveness of our multi-source self-supervised paradigm.

D. Downstream Classification Results

Across all downstream seeds, Vanilla MAE achieved a mean QWK of 0.4084, whereas ProsMAE achieved a higher mean QWK of 0.4736. This corresponds to an absolute improvement of 0.0652 QWK under the primary disjoint split. The averaged result was computed across seeds 42-52 for Vanilla MAE and seeds 42-51 for ProsMAE. Because the reported values are validation best QWK and the seed ranges are not fully paired, formal statistical significance testing is not claimed in this work.

These results indicate that multi-source histopathology MAE pretraining improves ordinal agreement under the current disjoint split and frozen linear probing. Although the validation set is relatively small and seed variance remains, the averaged results show a consistent improvement over the vanilla MAE baseline.

E. Ablation Study

To better understand the source of performance improvement, we conduct ablation studies on the mask ratio, noise injection, baseline split robustness, and tile sampling sensitivity.

1) *Mask Ratio*: We first compare MAE mask ratios of 0.25, 0.50, and 0.75 in Table III under the same disjoint split and 5000-step MAE pretraining setup.

TABLE III
MASK RATIO ABLATION RESULTS

Mask Ratio	Best QWK	Final QWK	Acc.	Macro-F1
0.25	0.3963	0.3781	0.3125	0.3042
0.50	0.4274	0.3774	0.3000	0.2875
0.75	0.4699	0.4656	0.2875	0.2902

Although the mask ratio of 0.25 achieves slightly higher accuracy, the 0.75 setting yields the highest Best QWK (0.4699) and Final QWK (0.4656). Because ISUP classification is an ordinal task, we prioritize QWK over standard accuracy to penalize larger grade discrepancies. Consequently, the 0.75 mask ratio is selected as our default pretraining configuration.

2) *Noise Injection*: Although the original hypothesis considered noise-robust MAE learning, the main ProsMAE setting uses no added noise. We evaluate whether Gaussian noise improves downstream performance using multiple noise levels in Table IV.

Noise injection does not consistently improve downstream QWK. Lower noise levels reduce performance, while noise level 0.20 achieves performance similar to the no-noise setting. Therefore, no-noise mask 0.75 is retained as the primary result, and noise injection is treated as a supporting robustness ablation rather than the central contribution.

TABLE IV
NOISE INJECTION ABLATION RESULTS
(MULTI-SOURCE, MASK RATIO = 0.75)

Noise	Best QWK	Std
w/o noise	0.4734	0.0104
0.02	0.3694	0.0477
0.05	0.3943	0.0513
0.10	0.4350	0.0225
0.20	0.4733	0.0184

3) *Split Sensitivity of the Vanilla Baseline*: To evaluate whether the vanilla MAE baseline is sensitive to the PANDA train-validation split, we repeat downstream evaluation across three independent disjoint splits in Table V using the same frozen linear-probe setting.

TABLE V
VANILLA MAE SPLIT ROBUSTNESS RESULTS

Split	Runs	Mean QWK	Std	Min	Max
43	3	0.2687	0.0286	0.2367	0.2918
44	3	0.4972	0.0340	0.4616	0.5294
45	3	0.3056	0.0159	0.2910	0.3225
Overall	9	0.3572	0.1088	0.2367	0.5294

As shown in Table V, vanilla MAE exhibits noticeable variation across disjoint PANDA splits, suggesting that downstream ISUP classification performance is sensitive to split composition under the current low-compute protocol. Therefore, the ProsMAE results should be interpreted as improvement under the primary disjoint split rather than as evidence of universal split-level superiority.

4) *Tile Sampling Sensitivity*: We further evaluate whether ProsMAE performance depends strongly on selecting exactly 100 tiles per slide during downstream feature extraction. Additional experiments are performed using 50 and 150 tiles per slide in Table VI.

TABLE VI
PROSMAE TILE SAMPLING SENSITIVITY RESULTS

Tiles/Slide	Runs	Mean QWK	Std	Min	Max
50	3	0.5039	0.0203	0.4856	0.5258
100 (main)	4	0.4734	0.0104	0.4613	0.4860
150	3	0.4817	0.0234	0.4607	0.5070

Although the 50-tile setting achieved a slightly higher mean QWK, 100 tiles showed the lowest standard deviation across repeated runs and was retained as the main setting because it was the pre-specified default in our experimental protocol. These results suggest that ProsMAE is not highly sensitive to the exact number of sampled tiles within the evaluated range.

IV. CONCLUSION

This paper presented ProsMAE for multi-source MAE pretraining and ProsCLS for downstream ISUP grade classifi-

caution. The proposed pipeline is designed as a low-compute and deployment-friendly framework, using only 5000 MAE pretraining steps, a frozen encoder, mean-pooled WSI features, and a lightweight linear probe for downstream classification. Under the primary disjoint PANDA split, multi-source pretraining improved mean validation QWK over the vanilla MAE baseline, while noise injection served as a supporting ablation rather than the main contribution. Because downstream evaluation is performed on a single PANDA cohort and primary split, broader robustness across external cohorts cannot yet be claimed. Future work will include repeated validation and evaluation on independent prostate cancer cohorts to verify generalization.

REFERENCES

- [1] H. Xu, N. Usuyama, J. Bagga, S. Zhang, D. Rao, T. Naumann, C. Wong, Z. Gero, J. González, Y. Gu *et al.*, “A whole-slide foundation model for digital pathology from real-world data,” *Nature*, vol. 630, no. 8015, pp. 181–188, 2024.
- [2] G. Campanella, M. G. Hanna, L. Geneslaw, A. Mirafior, V. Werneck Krauss Silva, K. J. Busam, E. Brogi, V. E. Reuter, D. S. Klimstra, and T. J. Fuchs, “Clinical-grade computational pathology using weakly supervised deep learning on whole slide images,” *Nature Medicine*, vol. 25, pp. 1301–1309, 2019.
- [3] M. Y. Lu, D. F. K. Williamson, T. Y. Chen, R. J. Chen, M. Barbieri, and F. Mahmood, “Data-efficient and weakly supervised computational pathology on whole-slide images,” *Nature Biomedical Engineering*, vol. 5, pp. 555–570, 2021.
- [4] W. Bulten, K. Kartasalo, P.-H. C. Chen, P. Ström, H. Pinckaers, K. Nagpal, Y. Cai, D. F. Steiner, H. van Boven, R. Vink *et al.*, “Artificial intelligence for diagnosis and gleason grading of prostate cancer: the panda challenge,” *Nature Medicine*, vol. 28, pp. 154–163, 2022.
- [5] G. Campanella, S. Chen, M. Singh, R. Verma, S. Muehlstedt, J. Zeng, A. Stock, M. Croken, B. Veremis, A. Elmas *et al.*, “A clinical benchmark of public self-supervised pathology foundation models,” *Nature Communications*, vol. 16, no. 1, p. 3640, 2025.
- [6] W. Chen *et al.*, “Beyond vit tokens: Masked-diffusion pretrained convolutional pathology foundation model for cell-level dense prediction,” *arXiv preprint arXiv:2605.08276*, 2026.
- [7] K. He, X. Chen, S. Xie, Y. Li, P. Dollár, and R. Girshick, “Masked autoencoders are scalable vision learners,” in *Proceedings of the IEEE/CVF Conference on Computer Vision and Pattern Recognition*, 2022, pp. 16 000–16 009.
- [8] A. Dosovitskiy, L. Beyer, A. Kolesnikov, D. Weissenborn, X. Zhai, T. Unterthiner, M. Dehghani, M. Minderer, G. Heigold, S. Gelly *et al.*, “An image is worth 16x16 words: Transformers for image recognition at scale,” in *International Conference on Learning Representations*, 2021.
- [9] M. Aubreville, N. Stathonikos, C. A. Bertram, R. Klopffleisch, N. ter Hoeve, F. Ciompi *et al.*, “Mitosis domain generalization in histopathology images – the midog challenge,” *Medical Image Analysis*, vol. 75, p. 102262, 2022.
- [10] D. Tellez, G. Litjens, P. Bandi, W. Bulten, J.-M. Bokhorst, F. Ciompi, and J. van der Laak, “Quantifying the effects of data augmentation and stain color normalization in convolutional neural networks for computational pathology,” *Medical Image Analysis*, vol. 58, p. 101544, 2019.
- [11] P. Bandi, O. Geessink, Q. Manson, M. Van Dijk, M. Balkenhol, M. Hermesen, B. E. Bejnordi, B. Lee, K. Paeng, A. Zhong *et al.*, “From detection of individual metastases to classification of lymph node status at the patient level: the camelyon17 challenge,” *IEEE transactions on medical imaging*, vol. 38, no. 2, pp. 550–560, 2018.
- [12] N. Brancati, A. M. Anniciello, P. Pati, D. Riccio, G. Scognamiglio, G. Jaume, G. D. Pietro, M. D. Bonito, A. Foncubierta-Rodríguez, G. Botti, M. Gabrani, F. Feroce, and M. Frucci, “Bracs: A dataset for breast carcinoma subtyping in h&e histology images,” *Database*, vol. 2022, p. baac093, 2022.
- [13] D. Wang, S. Han, Y. Xu, Z. Wu, L. Zhou, B. Morovati, and H. Yu, “Lomae: Simple streamlined low-level masked autoencoders for robust, generalized, and interpretable low-dose ct denoising,” *IEEE Journal of Biomedical and Health Informatics*, vol. 28, pp. 6815–6827, 2024.
- [14] T. Chen, S. Kornblith, M. Norouzi, and G. Hinton, “A simple framework for contrastive learning of visual representations,” in *Proceedings of the International Conference on Machine Learning*, 2020, pp. 1597–1607.
- [15] O. Ciga, T. Xu, and A. L. Martel, “Self supervised contrastive learning for digital histopathology,” *Machine Learning with Applications*, vol. 7, p. 100198, 2022.
- [16] J. Cohen, “Weighted kappa: Nominal scale agreement with provision for scaled disagreement or partial credit,” *Psychological Bulletin*, vol. 70, no. 4, pp. 213–220, 1968.
- [17] K. Takahashi, K. Yamamoto, A. Kuchiba, and T. Koyama, “Confidence interval for micro-averaged f1 and macro-averaged f1 scores,” *Applied Intelligence*, vol. 52, pp. 4961–4972, 2021.